Xin *et al. Environmental Systems Research* (2026) 15:1
https://doi.org/10.1186/s40068-025-00434-2

Environmental Systems Research

RESEARCH Open Access

Formation and characterization of water-in-oil emulsions: insights from simulated mesoscale oil spill tests

Qin Xin[1*], Christine Ridenour[2] and Hena Farooqi[1]

Abstract
Transporting oils across Canada via pipelines, rail, and tankers poses environmental risks from potential spills into waterways. Understanding how oil properties and environmental conditions influence the formation and stability of weathered water-in-oil (w/o) emulsions is critical. This study examines the spill behaviors of five oils—Hibernia Crude (HC), Alaska North Slope (ANS), Diluted Bitumen (Dilbit), Very Low Sulfur Fuel Oil (VLSFO), and Point Arguello Crude (PAC)—in saltwater under wave conditions using mesoscale spill tests. All oils exhibited rapid initial water uptake within 24 h and significant loss of light fractions due to evaporation. The resulting w/o emulsions exhibited increased density and viscosity over the 96-hour observation period. Their types and stabilities were influenced by water content and the composition of major subfractions remaining in the emulsions. These findings underscore the importance of understanding oil-specific properties and weathering processes to predict emulsion behavior and inform effective spill response strategies.

Keywords Oil chemistry, Spill behavior, Emulsification, Salt water, Wave condition

Introduction

Conventional and unconventional crude oils, along with fuel oils, are complex mixtures of hydrocarbons and other organic compounds, characterized by varying degrees of volatility, solubility, and dispersibility in water. When oil is spilled into an aquatic environment, it is immediately exposed to a range of biotic and abiotic weathering processes, including evaporation, spreading, drifting, dispersion, dissolution, emulsification, and oxidation (Royal Society of Canada 2015; Xin et al. 2023; Xin et al. 2024). W/O emulsification refers to the formation of emulsions in which water droplets are dispersed within a continuous oil phase, develop over time post-spill with the weathering process. Environmental factors such as mixing, water and air temperature, insolation levels, and indigenous microbes play a crucial role in the formation of water-in-oil (w/o) emulsions. Additionally, an oil's physical properties and chemical composition significantly influence its emulsification tendency and behavior in water (Royal Society of Canada 2015). These emulsions typically stabilized by natural or added emulsifiers, depending on the type of formed emulsions, which are usually kinetically stable but thermodynamically unstable. Overall, their formation and stability are influenced by multiple factors, including oil composition, environmental conditions (which include but limited to temperature and turbulence that varies both spatially and temporally), and the duration and presence of emulsifying agents. Emulsification significantly alters the physical

*Correspondence:
Qin Xin
Qin.Xin@NRCan-RNCan.gc.ca
[1]Natural Resources Canada, CanmetENERGY, 1 Oil Patch Drive, Devon, AB T9G 1A8, Canada
[2]Environment and Climate Change Canada, 9250 49 Street NW Edmonton, Alberta, Canada

properties of spilled oils, especially in viscosity and volume, and can pose substantial challenges to response and recovery floating oil residues during spill operations.

There is much research on w/o emulsion formation, classification, stability, chemical demulsification, and other aspects related to crude oil emulsification and thermodynamics, which is considered as a common issue in the oil and gas industry (Wong et al. 2015; de Oliveira et al. 2018; Wang et al. 2021; Abdulredha et al. 2022). W/O emulsions formed, e.g., in the production sites or pipelines are unwanted and have negative effects or problems to the field. Similarly, in the oil spill field, the formed w/o emulsions significantly influence the nature of oil spills at sea as well as clean-up response. Due to emulsification, the properties and characteristics of oil spills will alter to a significant extend, especially in the volume of spilled materials, density and viscosity of oil (Fingas and Fieldhouse 2004). Based on a series of lab-scale mixing tests, Fingas et al. classified w/o emulsions into four categories: stable, mesostable, entrained water, and unstable (Fingas and Fieldhouse 2009; Fingas 2014). This characterization was based on a series of rheological measurements, visual appearance, and water content over time. Stable emulsions typically have a high-water content (approximately 78 wt%) and retain most of this water for at least a year. Meso-stable emulsions contain approximately 65 wt% water but lose the majority within a few days of formation. Entrained w/o emulsions hold about 40 wt% water, which gradually separates from the oil phase over the course of a year. Unstable emulsions, by contrast, contain only a small percentage of water, which separates rapidly after formation. One well-known type of stable w/o emulsion, often referred to by oil spill responders as "chocolate mousse" or simply "mousse", is characterized by its high viscosity and semi-solid appearance.

From a compositional standpoint, extensive research has shown that asphaltenes act as the primary stabilizers of w/o emulsions, whereas resins enhance their stabilizing effect by solvating asphaltene molecules, preventing aggregation, and strengthening the interfacial film between oil and water (Fingas and Fieldhouse 2009; Rane et al. 2013; Wong et al. 2015; Muriel and Katz 2021). The formation of interfacial films by naturally occurring asphaltenes around water droplets facilitates the emulsification process. While resins also contribute to emulsion formation, they do not independently create stable emulsions. Instead, resins support asphaltenes by acting as solvents, providing temporary solution stability and aiding in the gradual migration of asphaltenes to stabilize the emulsion (Rane et al. 2013; Fingas 2014). Muriel and Katz have studied the time evolution and effect of dispersants on the morphology and viscosity of w/o emulsions using an overhead laboratory mixer with stirring at 660 rpm (for 22 h) in an open 4.0 L glass beaker. The increase in emulsion viscosity over 22 h has been attributed to changes in the interfacial rigidity and aggregation networks, as well as light oil's evaporation (Muriel and Katz 2021). Recent, Li et al. (2025) investigated the impact of below-freezing air temperatures on the formation and stability of w/o emulsions in seawater using an end-to-end rotator. Results showed w/o emulsion viscosity increased markedly and that low air temperatures will substantially affect the stability of emulsions, primarily through their effects on the entrained water droplets.

Water-oil mixing energy also plays a critical role in the formation of w/o emulsions. Fingas et al. (1999) conducted a preliminary investigation into the energy threshold required for emulsification using an end-over-end rotary mixing protocol. Their results indicated that the onset of stable and entrained emulsions occurs at very low energy levels, corresponding to rotational rates as low as 1–3 rpm. More recently, the emulsification behavior of various bitumen-derived products was examined using the same protocol (Xin et al. 2022; Hounjet et al. 2023). These studies demonstrated that the properties of the resulting floating w/o emulsions are influenced by the asphaltene content of the oil and its thermochemical processing history.

Beyond lab-scale testing, research has progressed to investigate the w/o emulsification process using mesoscale tank systems, which better simulate the combined weathering processes that occur following an oil spill. Daling et al. conducted a study examining the formation of w/o emulsions from MC 252 crude oil (a light paraffinic crude) in a mesoscale flume basin, under varying sea temperatures and wave conditions, and in the presence of dispersants. Their findings provided valuable insights into the evolution of w/o emulsion properties over time (Daling et al. 2014). The study revealed that during the initial days following the spill, an unstable, low-viscosity w/o emulsion typically formed under calm sea conditions. However, a more stable w/o emulsion could gradually develop over the course of several days (Daling et al. 2014). Recent studies have increasingly focused on the fate and behavior of various petroleum crudes in freshwater environments using mesoscale tank systems. In one such study, w/o emulsion formed 28 to 35 days after the spillage of Mixed Sweet Blend (MSW) conventional crude oil in a freshwater system contained over 66 wt% water and exhibited viscosities more than 200 times higher than that of fresh MSW (Lara-Jacobo et al. 2021; Xin et al. 2024). In contrast, entrained w/o emulsions formed 35 days after the spillage of diluted bitumen (Dilbit) in freshwater at two different temperatures contained 32–39 wt% water and similarly exhibited viscosities exceeding 200 times that of fresh Dilbit (Xin et al. 2023). Notably, the entrained w/o emulsions produced in mesoscale open-system tests differed significantly

from the stable, high-water-content w/o emulsions generated under closed-jar mixing conditions (Hounjet et al. 2023). This divergence may be attributed to the suppression of oil evaporation during closed jar mixing, as well as differences in mixing intensity and weathering duration. Additionally, the influence of wave energy and microbial activity following the spill contributed to the observed differences in emulsion characteristics under varying conditions (Heshka et al. 2021; Xin et al. 2023). Most recently, Muriel et al. examined the effects of wave energy and photo-oxidation on the emulsification process involving artificial seawater and crude oil. Their results showed that photo-oxidation significantly enhanced water uptake, promoted droplet clusters, reduced characteristic droplet size, and increased the dominance of the storage modulus, indicating a more elastic emulsion compared to the untreated Hibernia crude oil (Muriel et al. 2024).

The extent of oil emulsification is influenced by both the intrinsic properties of fresh oil and prevailing environmental conditions. The physicochemical characteristics of fresh water govern its initial behavior, including spreading, dispersion, dissolution, volatility, water uptake rate, and the formation and stability of w/o emulsions. Environmental factors such as turbulence, wind, solar radiation, microbial activity, and temperature also play critical roles in determining emulsion formation and evolution. However, variability in testing protocols and measurement techniques presents challenges in applying experimental data to model inputs or validation. Many laboratory protocols fail to replicate key field conditions, such as spreading and evaporation of volatile components. In contrast, mesoscale testing facilities provide significant advantages by allowing the simultaneous simulation of multiple oil weathering and transport processes under controlled wave energy conditions that mimic natural turbulence. These processes include the evaporation of volatiles, dispersion into the water column, and water uptake by floating oil, which are particularly influential during the early stages of a spill (within days) and critically affect w/o emulsion formation. As weathering progresses, oxidative processes such as photo-oxidation and biodegradation begin to transform oil components within w/o emulsions (Lee 2003), altering their chemical and physical properties. Compounds such as carboxylic acids, aldehydes, and polycyclic aromatic hydrocarbons undergo oxidation, generating polar functional groups. These transformations can impart surfactant-like properties to the oxidized compounds (Plata et al., 2008). The formation of surfactant-like compounds directly impacts the types and stability of w/o emulsions by modifying the microstructure of water droplets and promoting stable emulsion formation (Muriel & Katz 2023).

In this study, we selected five oils with distinct physicochemical properties and compositions to investigate their spill behaviors under consistent mesoscale environmental condition. This work encompassed the characterization of both the source oils and their resulting w/o emulsions, with the goal of advancing our understanding of emulsion formation mechanisms and stability. Five spill tests were conducted, with 2.0 L of each oil (four crude oils and one fuel oil) spilled onto 1,200 L saltwater at room temperature and allowed to weather for 96 h under wave mixing conditions. The experimental system was designed to enable key weathering processes such as oil spreading, evaporation, dispersion, dissolution, and emulsification. By evaluating emulsification tendencies, water content, viscosity changes, droplet characteristics, and emulsion stability, this microcosm approach allows us to gain insights for multiple crude oils and provides insights into how tested oil composition influences the formation, evolution, and persistence of w/o emulsions under controlled and relevant coastal environment condition.

Experimental section

Source oils, salt water and chemicals

Five types of oils, which included Hibernia Crude (HC, Newfoundland, CA), Alaska North Slope (ANS, Alaska, USA), Diluted Bitumen (Dilbit, i.e., Cold Lake Blend, Alberta, CA), Very Low Sulfur Fuel Oil (VLSFO, ExxonMobil, USA), and Point Arguello Crude (PAC, California, USA) were collected from various refinery suppliers in North America. Artificial salt water was prepared by dissolving sodium chloride in local tap water (Devon, AB, CA) to reach a 3.3 wt% concentration. All other chemicals and solvents, including carbon disulfide (CS_2) and dichloromethane (DCM, CH_2Cl_2), were purchased from Sigma Aldrich as "HPLC grade" and were used as received.

Mesoscale spill test protocol

Oil spill experiments were conducted using the mesoscale spill tank described previously (Xin et al. 2023; Saborimanesh et al. 2023; Xin et al. 2024). Briefly, a 316 stainless steel spill test tank (size: 3 m × 1 m × 1.5 m, L × W × H; water surface area: 2 m^2), contains a moving paddle at one end to create waves, while the other end is designed to simulate a shoreline (Fig. 1). Before each test, the mesoscale tank was filled with 1,200 L of artificial salt water to a height of 0.7 m and the water temperature was adjusted to 15 ˚C.

Each oil spill test lasted 96 h post-spill. Tests were initiated by pouring two liters of oil onto the water surface (equivalent to a 1 mm-thick oil slick) through a pouring device. During the tests, evaporation of water from the tank was compensated for by the addition of tap water

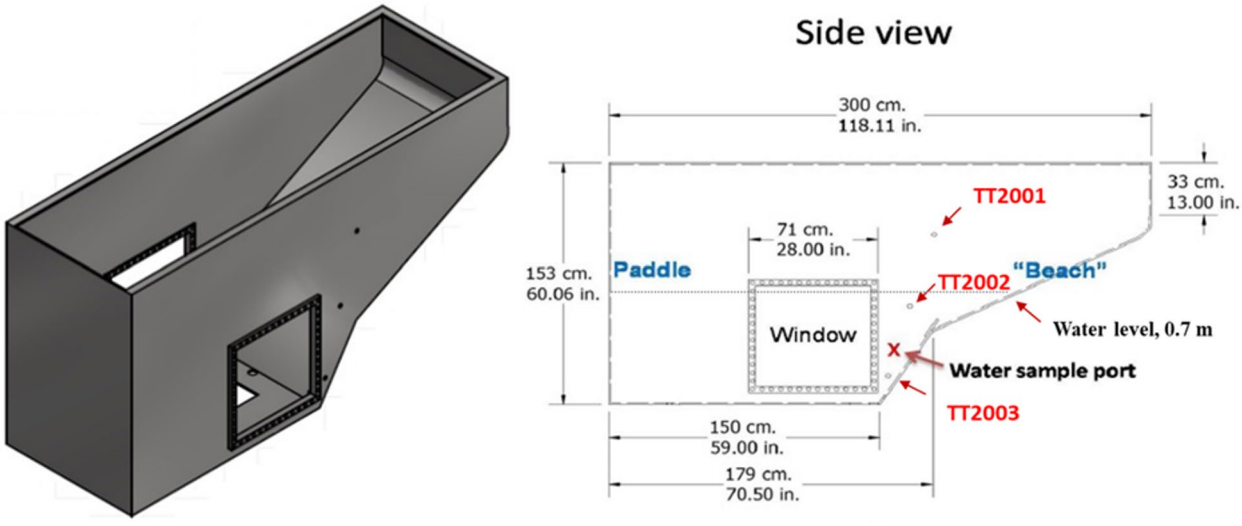

Fig. 1 Schematic of the spill tank. Temperature transmitters, TT2003 and TT2002, measure water temperature while TT2001 measures air temperature. The water sample port, which is a stainless-steel tube with a diameter of 6.35 mm (1/4 inch) located at a height of 0.3 m above the tank bottom and situated within the water column

to maintain a constant water height of 0.7 m. The wave-generating paddle was operated at 93 rpm for continuous surface mixing during the first 24 h to simulate high-wave condition, then turned off for the next 24 h to represent calm condition without wind or waves. This intermittent wave cycle pattern was repeated over each 96-h spill test to mimic the changes in nearshore coastal water conditions caused by tidal cycles. When the paddle was turned on, the wave motion pushed the oil to the shoreline end of the tank under the high wave energy. The waves were generated in the tank and the instantaneous velocities were measured at various locations using an Acoustic Doppler Velocimeter (ADV), and the measured velocities were then used to calculate the energy dissipation rate (ε) to investigate various natural environmental conditions. (Liu et al., 2023). The experimental results indicated that at a depth of 0.2 m below the water surface, ε reached a magnitude of 10^{-4} W/kg in the middle of the tank and 10^{-3} W/kg closer to the shoreline. For the wave condition in this study (0.7 m water level and 93 rpm rotation speed), ε reached 1.0 W/kg at the water surface near the beach region. The detailed calculations and results are described in a previous publication (Liu et al., 2023). As artificial salt water was used in the tests and there was no real or simulated sunlight source present, biodegradation and photo-oxidation of the spilled oil are assumed to be negligible.

Characterization of source oil and W/O emulsions

Each oil sample was thoroughly homogenized using a barrel roller prior to subsampling for a series of analyses. These analyses included measurements of density, viscosity, water content, pour point, Interfacial Tension (IFT), surface tension, distillation fraction content, and boiling point distribution. Detailed descriptions of the analytical methods are provided in Table S1.

During each 96-h test, emulsified oil samples were collected at regular intervals (3, 24, 48, 72 and 96-h) from the oil mat on the water surface for physical and chemical characterization (Table S1). For each time point, three subsamples were analyzed for water content using Karl Fisher (KF) titration, and for boiling point distribution using High Temperature Simulated Distillation (HTSD). Additionally, the 96-h emulsion sample from each test was distilled to separate the Initial Boiling Point (IBP)–204 °C fraction, water, and the heavier oil fraction (Boiling Point (BP) > 204 °C fraction).

Following the physical distillation of the source oil and emulsions, each distillation fraction was further characterized. The IBP–204 °C fraction was analyzed by detailed hydrocarbon analysis and elemental content. The BP > 204 °C fraction was analyzed for elemental contents (C, H, N, S, and O) and, where applicable (HC, ANS, and VLSFO), further processed to remove wax. The wax-free portion was then separated into Saturates, Aromatics, Resins, and Asphaltenes (SARA) subfractions for detailed analysis (Fig. 2 and Table S1).

Imaging and stability evaluation of W/O emulsions

To monitor changes in the oil throughout the tests, observations of the floating w/o emulsions at the water surface were recorded using an intrinsically safe camera (Smart-EX® 01). Images were captured from above the tank and through a side window at each sampling time. Additionally, the 24-h and 96-h emulsion samples were analyzed for density and viscosity at three temperatures

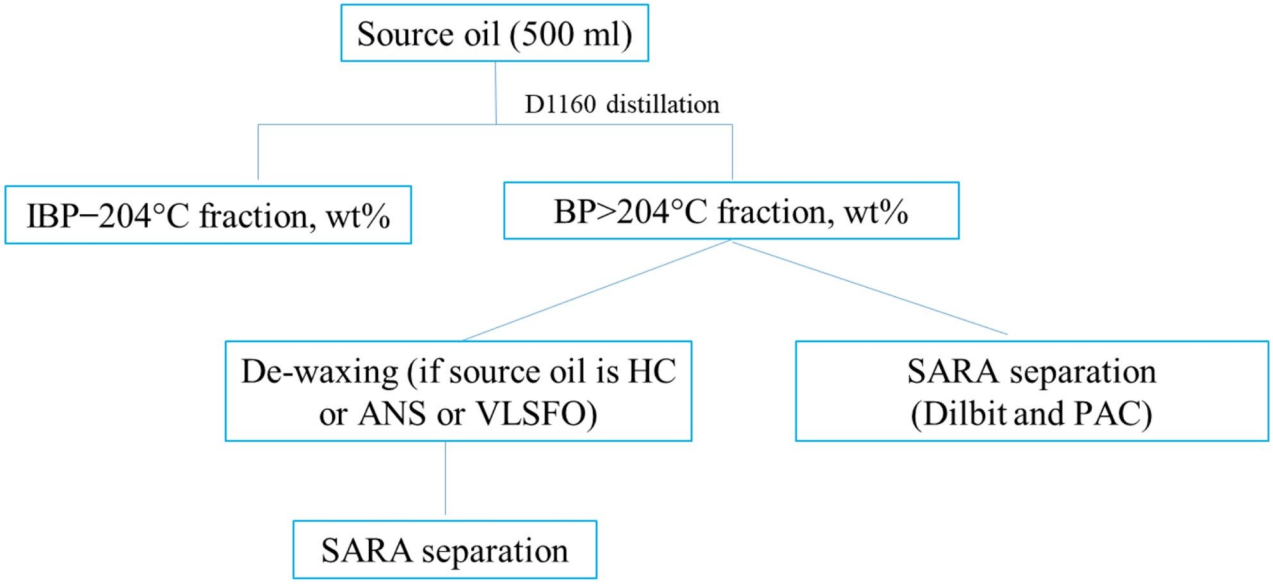

Fig. 2 Flowchart of source oil analyses, including the distillation, de-waxing and SARA separation processes

(Table S1), droplet size distribution using microscopic imaging, and emulsion stability.

A fluorescence microscope (Axio Imager.Z2M) equipped with a light source (X-Cite 120Q with 120 W Mercury Vapor Short Arc lamp), a filter (Alexa Fluor 488), a camera (AxioCam HR Rev3), and a Plan-Apochromat 40x/1.3 Oil DIC objective lens was used to analyze the size of water droplets within the emulsions. To minimize droplet deformation or diffusion during fluorescence microscopy, emulsion samples were imaged immediately after collection. A small drop of the sample was placed at the center of a glass slide between tape spacers, and a coverslip was gently applied to make light contact with the sample. Imaging was performed under low-intensity excitation and short exposure times to maintain droplet stability. For each subsample, thirty images were captured for droplet size analysis.

Rheological measurements were not conducted in this study and were not used to assess or predict emulsion stability. Instead, two methods were employed to assess the stability of the w/o emulsions. First, emulsion subsamples were placed in jars and left undisturbed for one week, during which visual observations were recorded to monitor phase separation. Second, pan spreading tests were conducted on the 24-h and 96-h emulsion samples following the protocol described by Zhao et al. (2022) (see Supplementary Information: Sect. "Introduction"), to confirm and validate the stability results obtained from the jar test. Zhao et al. recently observed that even highly "stable" emulsions formed in closed systems can undergo significant spreading when exposed to an open environment. The increased surface area available in open systems facilitates lateral spreading, which can lead to a reduction in apparent emulsion stability (Zhao et al. 2022).

Water sample collection and analysis

Water samples were collected from approximately mid-depth in the tank water column by opening a valve connected to a sampling port located 0.3 m from the bottom of the tank (as shown in Fig. 1) at three time points: before introducing oil (pre-spill), and at 3 and 96-h after the oil was introduced. The samples were filtered through 0.22 µm Nylon filters (Sigma-Aldrich) and analyzed for conductivity, pH, anions (Cl^-, HCO_3^{2-}), and major cations (Na^+, Mg^{2+}, K^+, Ca^{2+}).

Results and discussion

Oil properties

The five source oils exhibit diverse physical properties, as summarized in Table 1. At the three measured temperatures, a linear relationship was observed between oil density and temperature (°C) with an $R^2 > 0.9990$. A logarithmic relationship was calculated between viscosity and the inverse of absolute temperature (K^{-1}) with an $R^2 > 0.9971$.

Among the five oils analyzed, HC and ANS exhibited lower densities and viscosities compared to Dilbit, VLSFO and PAC, suggesting their relatively lighter and less viscous nature. These characteristics imply easier spreading and dispersion under spill scenarios, but potentially quicker evaporation and weathering processes. Conversely, the higher densities and viscosities of Dilbit, VLSFO, and PAC suggest that these oils may be more challenging to manage during spills, with slower spreading and potentially greater environmental

Table 1 Properties of source oils as received

Property	Unit	Method	HC	ANS	Dilbit	PAC	VLSFO
Density at 15 °C	g/mL	ASTM D7042	0.8590	0.8810	0.9199	0.9604	0.9675
Density at 20 °C	g/mL		0.8551	0.8775	0.9164	0.9572	0.9641
Density at 25 °C	g/mL		0.8513	0.8740	0.9129	0.9539	0.9603
R^2 (linear relationship)			0.9999	1.0000	1.0000	0.9999	0.9990
Viscosity at 15 °C	cP	ASTM D7042	14.1	17.2	214.7	1.4×10^4	3.7×10^3
Viscosity at 20 °C	cP		10.7	14.2	155.9	7.8×10^3	2.0×10^3
Viscosity at 25 °C	cP		8.6	11.9	115.8	4.6×10^3	1.1×10^3
R^2 (logarithmic relationship)			0.9971	1.000	0.9999	0.9995	0.9999
Water Content	wt%	Karl Fisher	0.01	0.03	0.34	4.09	0.16
Pour Point	°C	ASTM D97	0	−6	−33	−3	−9
IFT measurement at ambient temperature (23 °C)							
Air	mN/m	Du Noüy ring	26.1	26.3	27.4	29.7	N/A
Tap water*	mN/m		25.9 ± 0.2	10.6 ± 0.1	26.3	17.8	N/A
Salt water (3.3 wt% NaCl)#	mN/m		24.1	7.5 ± 0.1	23.9 ± 0.1	17.1	N/A

* surface tension of tap water is 71.5 mN/m;

surface tension of salt water is 72.7 mN/m;

N/A: not available (VLSFO is too viscous for the measurement)

persistence. Interestingly, Dilbit had the lowest pour point at −33 °C, while HC had the highest pour point at 0 °C, suggesting that HC is more prone to solidification under colder conditions. The highest pour point of HC is likely due to its moderately high wax content, significant saturate fraction, and low asphaltene fraction (in Table 3). The wax and possible long-chain paraffins in the saturates tend to crystallize and form a structured network, leading to an elevated pour point. PAC has the highest water content of 4.09 wt%. Interfacial Tensions (IFTs) with fresh and saltwater revealed notable differences among the oils. ANS had the lowest IFT values, suggesting a higher propensity for dispersion and interaction with the aqueous phase, which could influence its emulsification behavior. PAC followed ANS in terms of lower IFT values, while HC and Dilbit exhibited similar IFTs, reflecting comparable behaviors in their interaction with water.

The boiling point distributions of the five source oils are shown in Fig. 3, providing further insight into their composition and evaporation potential. The IBP–204 °C fraction, indicated by the blue dashed line, highlights significant differences among the oils. VLSFO contained the lowest proportion of this light fraction, with less than 2.0 wt%, followed by PAC at 12 wt%. In contrast, Dilbit, HC, and ANS exhibited comparable proportions of the IBP–204 °C fraction, ranging from 22.0 wt% to 25.6 wt%, making them relatively lighter oils. The BP > 524 °C fraction (vacuum residue), indicated by the red dashed line, showed PAC with the highest proportion, nearly 50 wt%, followed by Dilbit at 38 wt% and VLSFO at 37 wt%, underscoring their heavier composition. Conversely, HC and ANS had the lowest proportions of vacuum residue, at 20 wt% and 22 wt%, respectively, reinforcing their status as the lightest oils among the group.

These boiling point distributions align with the observed density and viscosity data (Table 1). HC and ANS, with the highest IBP–204 °C fractions and the lowest vacuum residue content, exhibited the lowest densities and viscosities, consistent with their lighter, more volatile nature. Conversely, PAC and VLSFO, with the smallest IBP–204 °C fractions and highest vacuum residue content, were the heaviest and most viscous oils in the group, reflecting their high concentration of heavy hydrocarbons. Dilbit, with intermediate values for both fractions, displayed properties between these extremes.

This distribution not only explains the physical properties but also highlights the distinct behavior these oils might exhibit during environmental weathering or spill response, where lighter fractions evaporate quickly and heavier fractions contribute to long-term persistence. Understanding these distributions is essential for predicting the fate of spilled oil and developing effective mitigation strategies.

Additionally, to enhance the prediction of evaporation behavior following a spill, the IBP–204 °C fractions of the five crudes were analyzed for their carbon number distribution (C_4–C_{12}) and hydrocarbon classes, including *n*-paraffins, isoparaffins, olefins, naphthenes, and aromatics. The results, presented in Figure S1, revealed a normal distribution of carbon numbers, with peaks around C_7–C_8 for most oils. Notably, Dilbit differed from the others by having the highest wt% of C_5, indicating a higher proportion of lighter hydrocarbons, which are more volatile and likely to evaporate rapidly post-spill. The saturates subfraction, comprising *n*-paraffins, isoparaffins, olefins, and naphthenes, constituted the majority

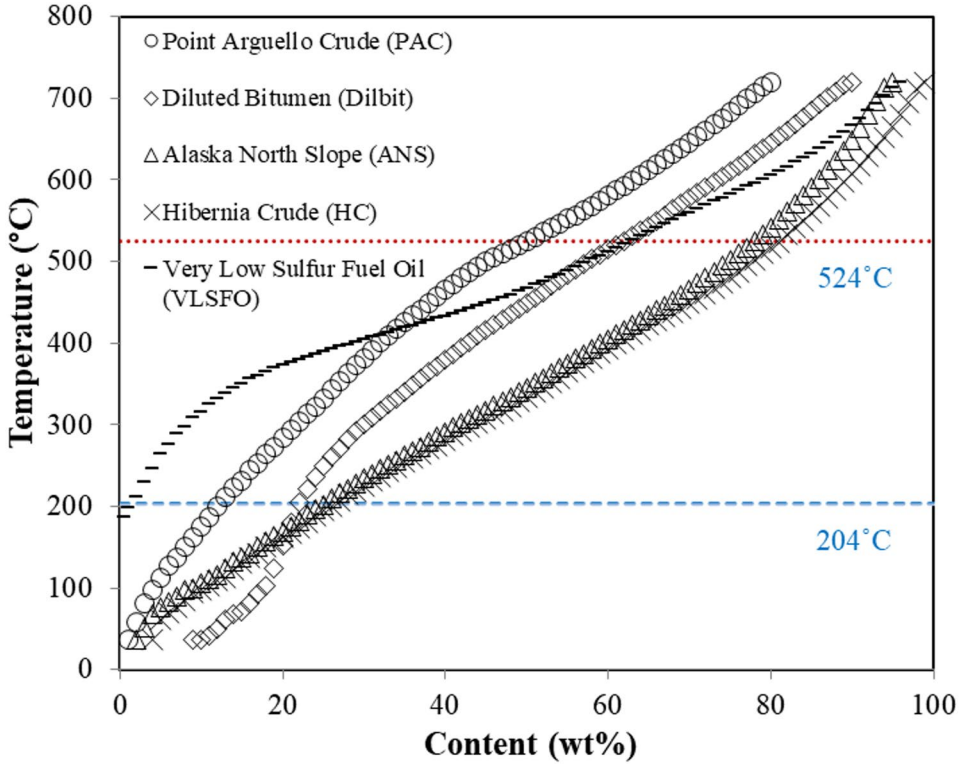

Fig. 3 Boiling point distributions of Point Arguello Crude (PAC, circle), Diluted Bitumen (Dilbit, diamond), Alaska North Slope (ANS, triangle), Hibernia Crude (HC, cross), Very Low Sulfur Fuel Oil (VLSFO, bar). The blue dashed line at 204 °C is plotted as a guideline to estimate the IBP–204 °C fraction of each oil, while the red dotted line at 524 °C is plotted as a guideline to estimate the > 524 °C fraction of each oil

Table 2 Water, saturates, aromatics, resins, asphaltenes contents normalized with respect to whole crude in fresh hibernia crude (HC), Alaska North slope (ANS), diluted bitumen (Dilbit), point Arguello crude (PAC), and very low sulfur fuel oil (VLSFO)

Subfraction	Unit	HC	ANS	Dilbit	PAC	VLSFO
Saturates*	wt%	60.0	54.3	38.4	25.8	36.4
Aromatics		29.4	29.0	32.8	30.0	43.3
Resins		10.3	15.0	15.2	16.2	14.6
Asphaltenes		0.3	1.8	13.6	23.8	5.5
Water		0.0	0.0	0.0	4.1	0.2

* The wax was included in the Saturates content

of the IBP–204 °C fraction's mass, highlighting the prevalence of relatively stable, nonpolar hydrocarbons in the lighter fractions. Within the residual aromatic hydrocarbons of the IBP–204 °C fraction, Benzene, Toluene, Ethylbenzene, and Xylenes (commonly known as BTEX compounds) dominated the aromatic class. These compounds are highly volatile, and their rapid evaporation can help mitigate long-term contamination but may pose significant risks to air quality immediately following a spill.

The CHNSO contents of the IBP–204 °C and BP > 204 °C fractions of the five source oils are shown in Table S2. The N, S, and O contents of the IBP–204 °C fractions were generally low or below the detection limit, indicating minimal heteroatom-containing compounds in the lighter fractions of these oils. In contrast, the BP > 204 °C fractions exhibited higher concentrations of N, S, and O for HC, Dilbit, PAC, and VLSFO. Among these, Dilbit and PAC contained the highest sulfur levels, suggesting a significant presence of sulfur-containing compounds in their heavier fractions. ANS was one exception, with negligible N, S, and O contents in both fractions, making it relatively simpler in composition and potentially less impactful from a heteroatom perspective during environmental weathering.

Normalized subfraction contents (including SARA and water) for the whole crudes are provided in Table 2. While the detailed SARA and wax contents in the BP > 204 °C fractions alongside the saturates and aromatics content in the IBP–204 °C fractions (extracted from Figure S1), are presented in Table 3.

Table 3 The contents of saturates, aromatics in IBP–204 °C fractions, the SARA and/or wax contents in the BP > 204 °C fractions, and contents of water in fresh (Hibernia crude (HC), Alaska North slope (ANS), diluted bitumen (Dilbit), point Arguello crude (PAC), and very low sulfur fuel oil (VLSFO)

Subfraction		Unit	HC	ANS	Dilbit	PAC	VLSFO
Saturates	IBP–204 °C	wt%	20.0	18.5	18.0	9.3	0.1
Aromatics			2.2	3.9	0.9	2.1	0.7
Saturates	BP > 204 °C		34.8	32.8	20.5	16.6	25.4
Aromatics			27.1	25.1	31.9	27.9	42.7
Resins			10.3	15.0	15.2	16.2	14.6
Asphaltenes			0.3	1.8	13.6	23.8	5.5
Wax			5.2	2.9	0.0	0.0	10.8
Water			0.0	0.0	0.0	4.1	0.2

Table 4 Summary of the visual observations from the five tank tests

Oil type	Visual observations	Post-spill, oil surface area*		
		24 h (waves off)	72 h (waves off)	Waves on
HC	Figures S2-3	1.0 m^2	0.7 m^2	For all oils, an oil mat was observed around the shoreline.
ANS	Figures S4-5	2.0 m^2	1.3 m^2	
Dilbit	Figures S6-7	1.0 m^2	0.7 m^2	
PAC	Figures S8-9	1.0 m^2	0.7 m^2	
VLSFO	Figures S10-11	0.7 m^2	0.2 m^2	

*Area error ± 0.1 m^2

Among the five oils, PAC contained the highest amounts of asphaltenes and resins (40 wt%), followed by Dilbit (28.8 wt%) and VLSFO (20.1 wt%). Despite its moderate asphaltene and resin content, VLSFO had the lowest content of the IBP–204 °C fraction (0.8 wt%) and the highest wax content (10.8 wt%), making it comparable to PAC as one of the heaviest crudes in terms of density and viscosity (Table 1). Dilbit exhibits lower density and viscosity than VLSFO and PAC, attributable to its higher IBP–204 °C fraction (18.9 wt%) and wax-free composition. In contrast, HC and ANS, characterized by the highest IBP–204 °C fractions, moderate wax and resin contents, and very low asphaltene levels, were classified as the two lightest crudes. The low asphaltene content in HC and ANS, despite the presence of wax and resins, significantly contributed to their lower density and viscosity, making them the lightest oils in the group (Table 1).

These differences underscore the influence of compositional variations—particularly the relative proportions of asphaltenes, resins, wax, and lighter fractions—on the physical properties and classification of crude oils.

Water-in-oil emulsion formation

A total of five 96-hour mesoscale tank tests were conducted, maintaining an average water temperature of 15 °C and an average air temperature of 18 °C. Each test involved 2.0 L of HC, ANS, Dilbit, PAC, or VLSFO introduced into 1,200 L of saltwater. During the tests, when the paddle was activated, the floating oil was subjected to the mixing forces of breaking waves. Conversely, when the paddle was turned off, the oil spread across the water surface. The properties of the artificial saltwater before and after oil contamination are summarized in Table S3. Concentrations of CO_3^{2-} and OH^- were consistently below the method detection limit for all samples and are therefore not included in the table.

Visual observations from the w/o emulsion formation during the five tests are shown in Figures S2-11, with a summary of observed oil surface area provided in Table 4.

Figures S2 and S4 present select images taken from above the tank during the HC and ANS tests, illustrating the time evolution of the oil's appearance on the water surface. Figures S3 and S5 show corresponding side-window images. Overall, HC and ANS exhibited similar behavior during the spill tests. Both oils were dispersed readily into the water column under wave action. Visual observations showed a darker water column for HC and ANS compared to the other three oils, likely due to their lower density and viscosity, which promoted the formation of a large number of subsurface oil droplets from wave-induced breakup. Three hours after the start of the tests, an oil mat began forming near the shoreline, and the water color lit as oil droplets resurfaced. When the motor was off at 24 and 72 h, the water surface was partially covered with oil, and the estimated surface area covered by floating oil is provided in Table 4. During periods of wave generation, the bulk of the floating oil mat was pushed against the sloped shoreline. In the later stages of the tests (48–96 h), the water became clearer, likely due to a reduced tendency for the oil to disperse into the water column under the same wave dispersion energy. This change was attributed to the increased viscosity of the w/o emulsion caused by the weathering process. This highlights the dynamic interplay between oil properties and environmental conditions during the progression of an oil spill.

Figures S6, S8, and S10 display select images taken from above the tank during the Dilbit, PAC, and VLSFO tests, illustrating the time evolution of the oil's appearance on the water surface. Corresponding images taken

from the side window are shown in Figures S7, S9, and S11. Compared to HC and ANS, the water column at the start of these tests appeared less dark for Dilbit, PAC, and VLSFO. This difference is likely due to the higher density and viscosity of these oils, which reduced their tendency to disperse and form droplets in the water column. Three hours into the tests, the oil mat was pushed by wave action toward the sloped shoreline. Unlike HC and ANS, the water column remained relatively clear throughout the Dilbit, PAC, and VLSFO tests, reflecting a lower degree of oil dispersion. Similar to the HC and ANS tests, wave generation caused the bulk of the floating oil mat to accumulate along the sloped shoreline, while periods with the motor off allowed the oil mat to spread out, partially covering the tank's surface area (Table 4). Among the tested oils, ANS exhibited the greatest spreading tendency during motor-off periods, while VLSFO showed the least. This difference in spreading behavior reflects the varying physical properties of the oils, particularly their viscosity and surface tension. To further explore the properties of the w/o emulsions formed during these spill tests, the characterization and stability analysis of the emulsions are detailed in Sect. "Water-in-oil Emulsion Characterization".

Water-in-oil emulsion characterization

Physical and chemical properties

The water content and boiling point distribution of the w/o emulsions were monitored at different time points throughout the tests to evaluate the emulsification process. Water was rapidly incorporated into the floating oil slick, with water content peaking at 24 h (Fig. 4). By the end of the 96-h test, the HC, ANS and VLSFO emulsions contained the highest water content (~ 60–70 wt%), followed by the Dilbit emulsion (~ 45 wt%) and the PAC emulsion (~ 29 wt%). The water uptake rate of HC was slightly slower than for ANS during the first 24 h, consistent with findings reported by Muriel et al. (2024). Figure 5 illustrates the loss of volatile compounds from the oils over time, as calculated from the boiling point

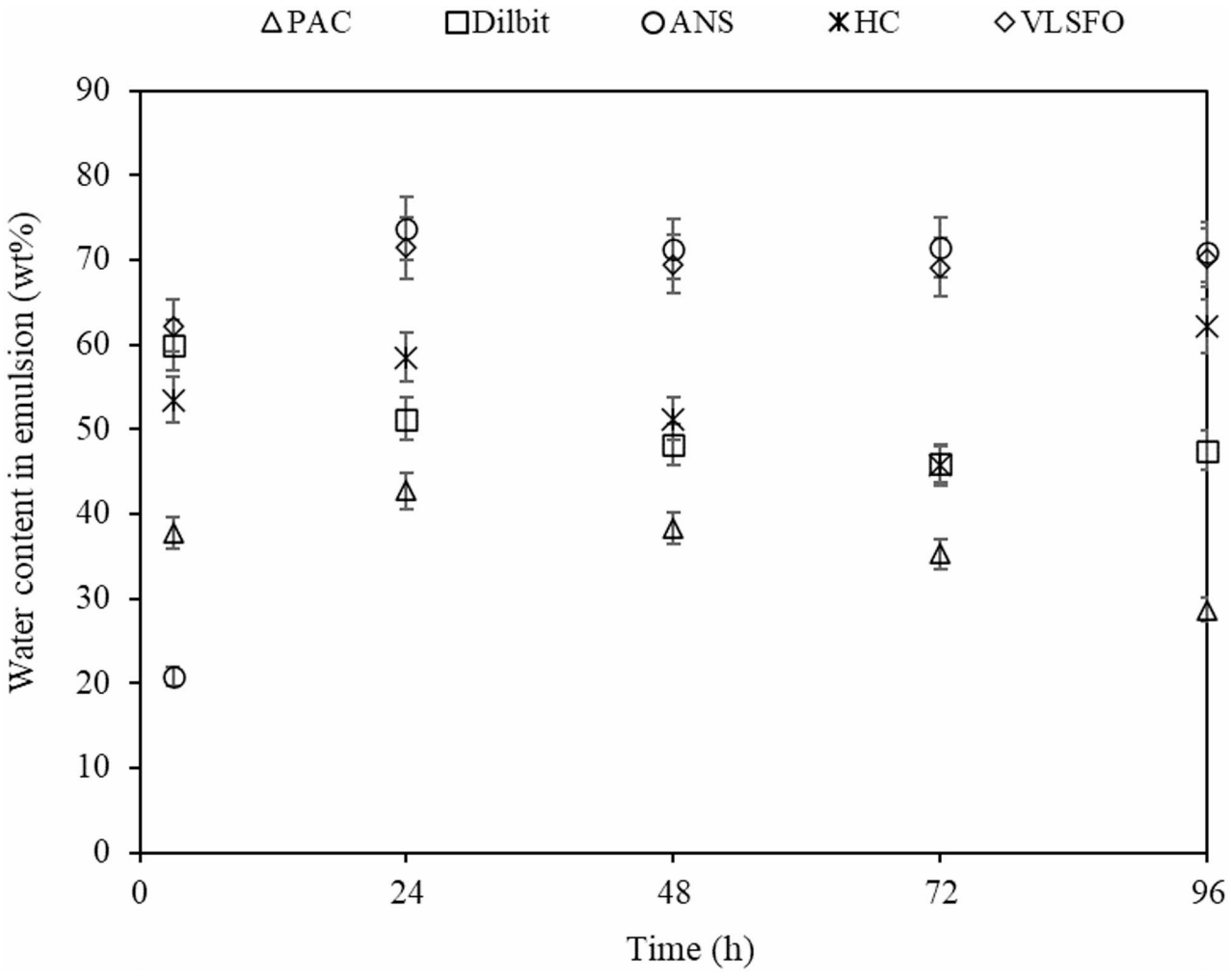

Fig. 4 Time evolution of water content of the weathered floating oils. The water content was measured by Karl Fisher titration

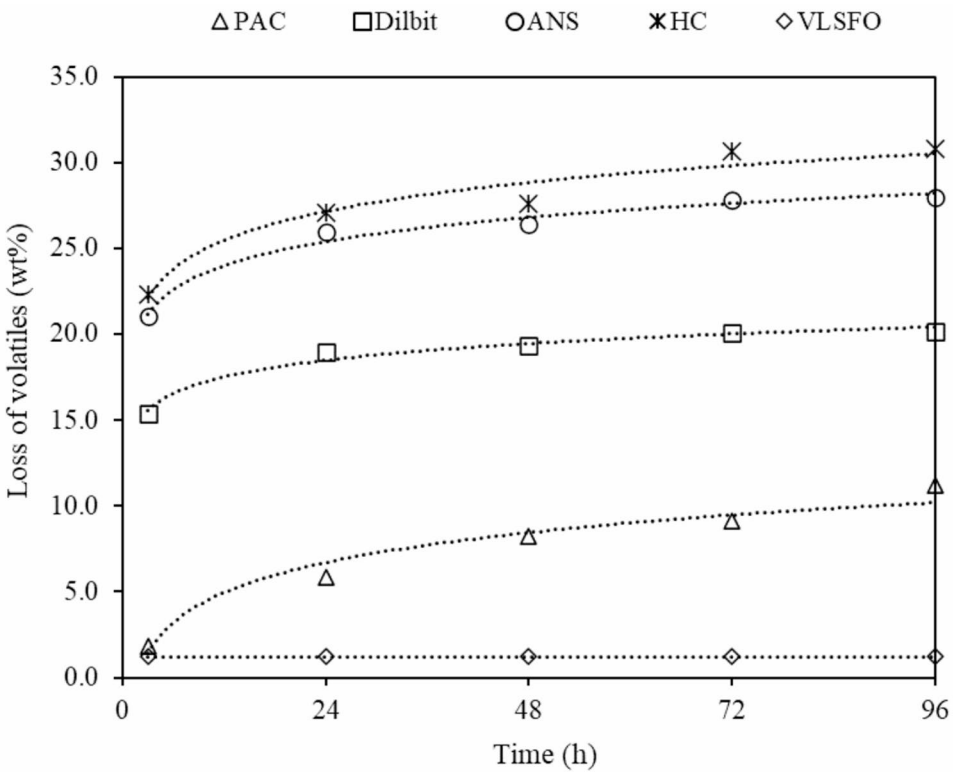

Fig. 5 Loss of volatiles from floating oils over time, calculated based on the measured high-temperature simulated distillation data of emulsion samples taken at different time points. The dotted lines represent best-fit logarithmic relationships between data points

Table 5 Summary of the physical and chemical properties of fresh oils and their corresponding water-in-oil emulsions from 24 h and 96 h

Oil/Emulsion	Oil Evaporation	Water content	Density	Viscosity		Saturates	Aromatics	Resins	Asphaltenes	Ratio of A/R*	Calculated	Predicted Stability
	wt%	wt%	g/mL (15°C)	mPa.s (30°C)	shear rate, s^{-1}	wt%	wt%	wt%	wt%		Stability Index	Type
HC	0.0	0.0	0.8590	6.7	N.A	60.0	29.4	10.3	0.3	0.03	29.7	Stable
HC, 24 h	27.1	58.5	0.9276	99.0	60.00	NA	NA	NA	NA	NA		
HC, 96 h	30.8	62.2	0.9396	179.0	34.00	52.8	29.0	16.9	1.3	0.1	2.8	Meso-stable
ANS	0.0	0.0	0.8810	10.0	N.A	54.3	29.0	15.0	1.8	0.1	15.9	Stable
ANS, 24 h	26.0	73.7	1.0000	4.9×10^3	1.36	NA	NA	NA	NA	NA		
ANS, 96 h	28.0	70.9	0.9980	4.9×10^3	1.36	41.4	30.6	18.3	9.7	0.5	-0.5	Meso-stable
Dilbit	0.0	0.0	0.9199	86.2	N.A	38.4	32.8	15.2	13.6	0.9	16.2	Stable
Dilbit, 24 h	18.9	51.3	1.0040	5.62×10^4	0.17	NA	NA	NA	NA	NA		
Dilbit, 96 h	20.2	47.5	1.0010	1.09×10^5	0.14	23.9	38.2	17.2	20.7	1.2	-5.2	Meso-stable
PAC	0.0	4.1	0.9604	2681.8	N.A	25.8	30.0	16.2	23.8	1.5	3.3	Entrained
PAC, 24 h	5.9	42.7	0.9864	6.6×10^4	0.21	NA	NA	NA	NA	NA		
PAC, 96 h	11.2	28.7	1.0020	2.1×10^5	<0.21	15.0	38.5	20.1	26.5	1.3	-10.1	Entrained
VLSFO	0.0	0.2	0.9675	627.8	N.A	36.4	43.3	14.6	5.5	0.4	3.3	Entrained
VLSFO, 24 h	1.2	71.4	0.9950	$4.4\times10^{3\ \#}$	2.80	NA	NA	NA	NA	NA		
VLSFO, 96 h	1.2	70.2	0.9986	$4.8\times10^{5\ \#}$	0.034	33.4	43.5	16.0	7.1	0.4	-12.3	Entrained

*A/R = Asphaltenes/Resins; # measured at 50 °C; NA: not available

distribution obtained via HTSD analysis. The IBP–204 °C fraction of the emulsions collected at different time points, derived from their boiling point distribution data, was compared with that of the corresponding fresh oil to quantify the loss of volatile components during weathering. A logarithmic relationship was observed between mass loss and time, highlighting the progressive evaporation of volatile compounds. The total mass loss of oil compounds from HC and ANS exceeded their initial IBP–204 °C fraction content, indicating that some compounds from the BP > 204 °C fraction were also lost during the 96-h weathering process. The mass loss of oil compounds for Dilbit and PAC was approximately equal to their IBP–204 °C fraction contents.

Table 5 summarizes the physical and chemical properties of fresh source oils and their resulting w/o emulsions

collected from the tank water surface after 24 h and 96 h of weathering. After 24 h of weathering, both the density and viscosity of the w/o emulsions increased significantly compared to their source oils. These changes were primarily attributed to the loss of volatile compounds from the oil and the uptake of water into the oil. However, between 24 and 96 h, no significant increase in emulsion density was observed. In contrast, apart from ANS oil, the non-Newtonian viscosities of the 96-h emulsions for the other four oils were more than twice those of the 24-h emulsions, indicating progressive weathering, as evidenced by the increased oil evaporation (wt%). Regarding the water content of the 96-h emulsions, PAC oil produced the lowest value (28.7 wt%). This was followed by the Dilbit emulsion (47.5 wt%), the HC emulsion (62.2 wt%), and the ANS and VLSFO emulsions, which exhibited the highest water contents at 70.2 wt% and 70.9 wt%, respectively.

In the last five columns of Table 5, the four SARA subfractions and the asphaltene-to-resin (A/R) ratio of the 96-hour emulsions are compared to those of the source oils. The saturate content generally decreased in the emulsions, while the relative proportions of resins and asphaltenes increased. The aromatic content of Dilbit and PAC also showed a slight increase, whereas the other three oils likely experienced a significant loss of semi-volatile aromatics during weathering. This trend aligns with the evaporation of volatile components, which are primarily composed of saturates and mono-ring aromatics (as shown in Figure S1). In particular, the amounts of semi-volatile aromatic compounds in HC, ANS, and VLSFO were likely higher than those in Dilbit and PAC, and were subsequently lost over time through evaporation or dissolution into the water column. Interestingly, for three of the oils (HC, ANS and Dilbit), the A/R ratio in the 96-h emulsions was higher than in the source oil. This suggests not only the loss of saturate and aromatic sub-fractions, but also the potential chemical transformation of asphaltenes and resins during the weathering process.

A comparison of the elemental contents of the BP > 204 °C fractions from the source oils and the 96-h emulsion samples (Table S2 & S4) revealed a slight increase in oxygen content after weathering. This provides additional evidence that chemical changes occurred in the oil compounds during the weathering process, likely driven by oxidation reactions that introduced polar oxygenated functional groups. These transformations, along with shifts in the A/R ratio, underscore the influence of weathering and water uptake on the evolution of w/o emulsions over time. To further assess the stability of the formed emulsions, analyses of water droplet size distributions and pan spreading behavior were performed. The results of these assessments are presented in the following section, offering a more comprehensive evaluation of emulsion behavior and stability under the test conditions.

W/O emulsion stability analyses

There are several methods to evaluate the stability of w/o emulsions. Subsamples of emulsions collected at 24 h and 96 h from each tank test were subjected to various analyses to characterize their properties and behavior. These included visual observation in jars, microscopic examination, and a pan spreading test designed to simulate an open saltwater environment. The pan spreading test followed the system developed by Zhao et al. (2022), providing a comprehensive evaluation of the emulsions' stability under conditions mimicking real-world scenarios. These combined methods offered valuable insights into the structural and behavioral stability of the emulsions formed during the tests.

Two microscope images of the 24-h and 96-h emulsion samples collected from the HC test are presented in Fig. 6-a. The observed dispersed water droplet sizes ranged from 1 μm to > 50 μm, with a low density of water droplets in both emulsions. This observation was inconsistent with the high-water content measured by KF titration for both emulsions (58.5 wt% and 62.2 wt%, as shown in Table 5). Visual observations of the emulsions sitting in jars (Figure S12) revealed that water had separated from both emulsions within one week, indicating their instability. This suggests that the water droplets incorporated into the spilled oil during the first 24 h were not effectively stabilized, likely due to the low A/R ratio of the HC oil. As a result, the droplets aggregated, coalesced, and eventually separated from the continuous oil phase. The pan spreading test further confirmed the instability of these emulsions, as both samples rapidly spread into thin surface sheens and disappeared within one minute (Figure S13).

The microscope images of the ANS w/o emulsion samples revealed a similar water droplet size distribution to the HC emulsions but with a higher density of water droplets (Fig. 6-b). Both the 24-h and 96-h ANS emulsions exhibited similar water droplet size distributions and high-water content (73.7 wt% and 70.9 wt%, respectively). Large, non-spherical water droplets were observed in the 24-h emulsion, reflecting incomplete stabilization at that stage. The viscosity of the 24-h and 96-h ANS emulsions was more than two orders of magnitude greater than that of fresh ANS oil. Despite the low A/R ratio in fresh ANS, which typically does not promote emulsion stability, the 96-h ANS emulsion displayed significant stability, with negligible water loss during a week-long visual observation (Figure S14). This enhanced stability is likely due to the higher asphaltene content (9.7 wt% for ANS vs. 1.3 wt% for HC) and a higher A/R

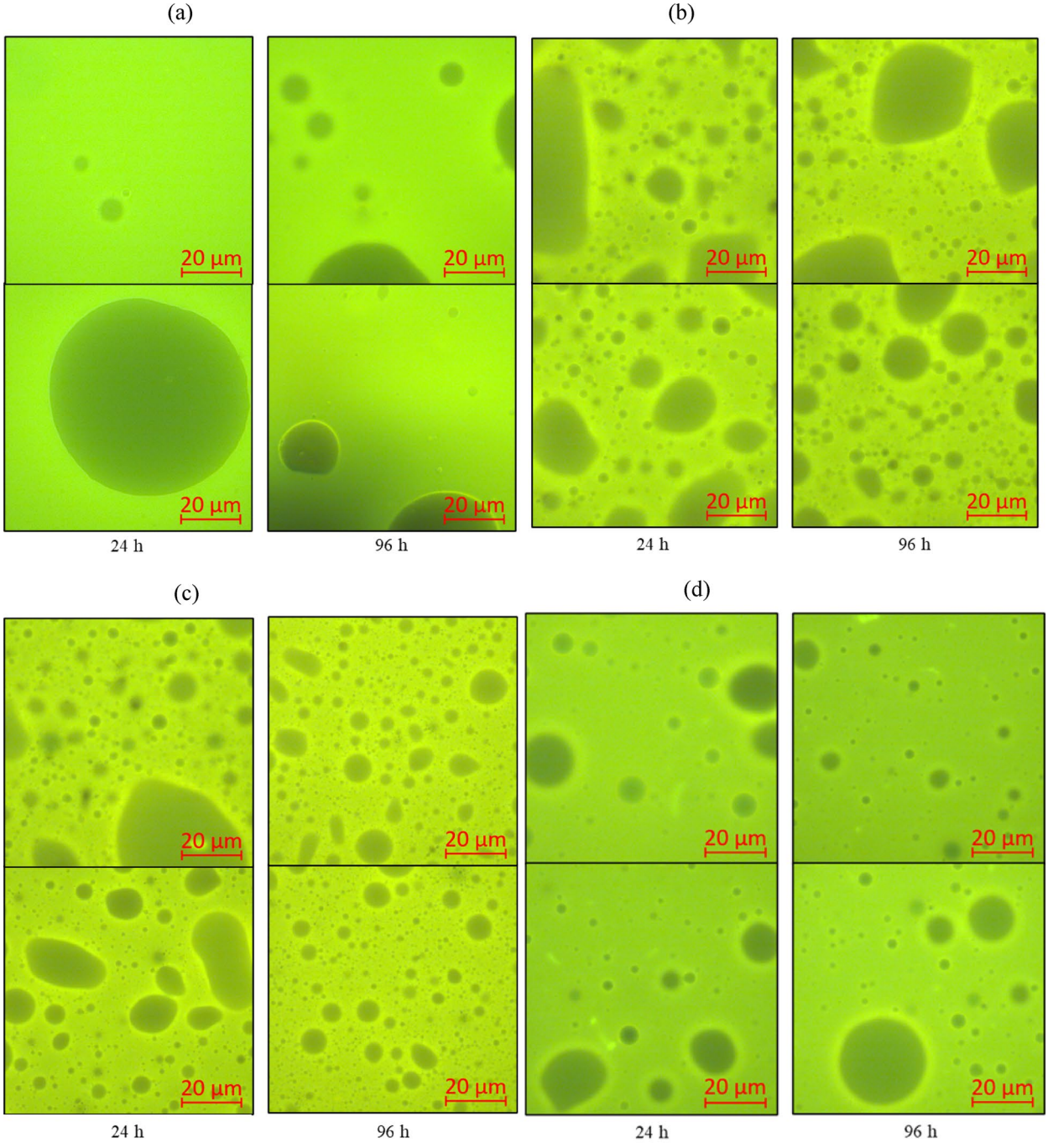

Fig. 6 Microscopy images of the 24-h and 96-h water-in-oil emulsions collected from the (**a**) Hibernia Crude; (**b**) Alaska North Slope; (**c**) Diluted Bitumen; (**d**) Point Arguello Crude; and (**e**) Very Low Sulfur Fuel Oil mesoscale tank tests; the grey circles indicate water droplets

ratio (0.5 for ANS vs. 0.1 for HC) in the ANS emulsions (Table 5). These findings suggest that the 96-h ANS emulsion formed a more stable structure compared to the HC emulsions. However, both the 24-h and 96-h ANS emulsions spread rapidly, forming thin sheens within one minute during the spreading tests (Figure S15).

Two microscope images of the 24-h and 96-h w/o emulsion samples collected from the Dilbit test revealed water droplet sizes ranging from 1 µm to 40 µm (Fig. 6-c). Fewer large water droplets were observed in the 96-h emulsion, indicating that large droplets in the first 24 h were lost over time. With further weathering, the emulsion evolved into a more stable form containing only small water droplets (< 15 µm), reflecting structural changes as weathering progressed. The water contents of the 24-h and 96-h emulsions were similar (~ 50 wt%),

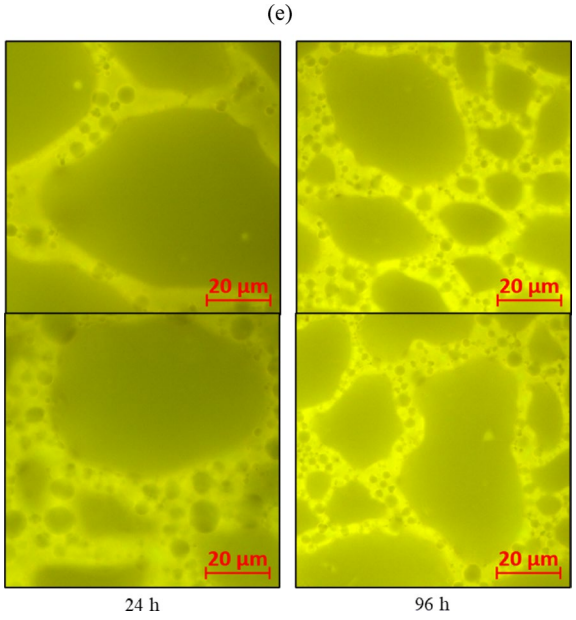

Fig. 6 (continued)

which is below the threshold for stable emulsions, typically characterized by water contents exceeding 78 wt%. During the visual observation test, the high-viscosity Dilbit emulsions coated the jar walls, preventing clear observations of water separation over the one-week period. The density and viscosity of both the 24-h and 96-h emulsions increased significantly compared to fresh Dilbit, indicative of the effects of weathering and water uptake. Unlike fresh HC and ANS, fresh Dilbit required more than one minute to fully spread and produce a sheen during the spreading test, reflecting its higher viscosity. For the 24-h and 96-h emulsions, it took over ten minutes to fully spread out (Figure S16), further demonstrating the impact of high viscosity on spreading behavior. This delayed spreading aligns with the general trend of increased emulsion stability as viscosity rises.

Two microscope images of the 24-h and 96-h w/o emulsion samples from the PAC test revealed water droplets distributed across a wide size range of 1 µm to 30 µm (Fig. 6-d). A medium-to-low density of water droplets was observed in both emulsions, consistent with the relatively low measured water contents (30 ~ 40 wt%). These water contents fall well below the threshold for stable emulsions, aligning with the lower degree of water incorporation observed in PAC. Interestingly, fresh PAC, despite having the highest viscosity among the five fresh oils, spread fully and very quickly within 1 min during the spreading test. However, spreading behavior slowed significantly as the emulsions weathered. The 24-h emulsion took approximately 5 min to fully spread, while the 96-h emulsion did not fully spread even after 15 min (Figure S17).

Two microscope images of the 24-h and 96-h w/o emulsion samples collected from the VLSFO test revealed water droplets distributed across a wide size range of 1 µm to > 60 µm (Fig. 6-e). A very high density of water droplets was observed in both emulsions, consistent with the high-water content measured by KF titration (~ 70 wt%, Table 5). The presence of large and irregularly shaped water droplets suggests entrainment, likely due to the high viscosity of VLSFO and the formation of a strong interfacial layer or network, potentially stabilized by asphaltenes and resins. Interestingly, the pan spreading tests showed that fresh VLSFO remained intact on the water surface for over 12 min without forming a sheen (Figure S18). This behavior is unusual, as it is not fully attributable to viscosity alone, since fresh VLSFO had the second-highest viscosity among the five oils. The medium-to-high asphaltene content and comparable resin levels did not explain the lack of spreading either. Instead, the reduced spreading is likely due to VLSFO's high wax content (10.8 wt%), which can hinder the solvation and mobility of hydrocarbons. Additionally, VLSFO's very low content of light and volatile compounds (IBP–204 °C fraction) likely contributed to the lack of spreading. These lighter fractions typically facilitate the solvation and dispersion of heavier hydrocarbons (BP > 204 °C fraction) on the water surface. The VLSFO emulsions, as expected, barely spread during the tests as well.

A summary of the water content, water droplet size distribution, pan spreading test results, and emulsion stability classification is presented in Table 6. Under this high-wave energy mesoscale test conditions, most oils formed similar types of emulsions within 24 h and at 96 h, with the exception of PAC. This observation aligns with the significant physical and chemical changes observed during the first 24 h, including the loss of volatile components and rapid water uptake. Emulsion stability is also strongly influenced by key aspects of oil composition, particularly the asphaltene and wax contents. These results underscore the dynamic behavior of spilled oil in aquatic environments and highlight the importance of considering the combined effects of weathering processes—including evaporation, oxidation, and microbial activity—when evaluating w/o emulsion formation, stability, and environmental fate. Future studies should focus on further understanding the individual and combined contributions of weathering processes to more accurately characterize and predict the behavior of w/o emulsions under real-world spill scenarios (Lara-Jacobo et al. 2021; Aeppli et al. 2022; Xin et al. 2023). Varying environmental conditions—such as solar radiation, microbial activity, and lower temperatures—should be taken into consideration. Advancing our understanding of these factors will help enhance response strategies

Table 6 A summary of w/o emulsion stability evaluation and stability type

Oil/Emulsion	Water content	Water droplet size		Fully spreading	Actual Stability
	wt%	density	μm	min	Type*
HC	0.0			Within 1.0 min	
HC, 24 h	58.5	low	1 μm to > 50 μm	Within 1.0 min	Entrained
HC, 96 h	62.2	low	1 μm to > 50 μm	Within 1.0 min	Entrained
ANS	0.0			Within 1.0 min	
ANS, 24 h	73.7	high	1 μm to > 50 μm	Within 1.0 min	Entrained
ANS, 96 h	70.9	high	1 μm to > 50 μm	Within 1.0 min	Entrained
Dilbit	0.0			Within 5 min	
Dilbit, 24 h	51.3	high	1 μm to 40 μm	More than 10 min	Stable
Dilbit, 96 h	47.5	high	1 μm to 15 μm	More than 10 min	Stable
PAC	4.1			Within 1.0 min	
PAC, 24 h	42.7	medium	1 μm to 30 μm	Within 5 min	Meso-stable
PAC, 96 h	28.7	medium	1 μm to 30 μm	More than 15 min	Stable
VLSFO	0.2			More than 12 min	
VLSFO, 24 h	71.4	high	1 μm to > 60 μm	More than 12 min	Stable
VLSFO, 96 h	70.2	high	1 μm to > 60 μm	More than 12 min	Stable

*Classification: (1) Entrained emulsion: spreading < 1 min; (2) Meso-stable emulsion: spreading 1–10 min; (3) Stable emulsion: spreading > 10 min or no spreading

and more effectively mitigate the environmental impacts of oil spills across a broad range of aquatic conditions.

Conclusions

Five oils with distinct physical and chemical properties were tested for their emulsification tendencies and emulsion stability using a mesoscale tank test protocol. The five types of oil included Hibernia Crude (HC), Alaska North Slope (ANS), Diluted Bitumen (Dilbit), Point Arguello Crude (PAC), and Very Low Sulfur Fuel Oil (VLSFO). HC and ANS were classified as waxy light crude oils, characterized by their lower densities and viscosities (Table 1). Dilbit, a medium crude oil, exhibits intermediate density and viscosity properties due to its significant IBP–204 °C fraction (18.9 wt%), which acts as a diluent, reducing viscosity and enhancing flow characteristics. PAC and VLSFO were heavy crude oils, with VLSFO distinguished by its high wax content (10.8 wt%) and minimum diluent (0.8 wt%).

Under the same test conditions in an artificial saltwater environment, several common features were observed during the emulsification processes for all oils: (1) the initial water uptake occurred very rapidly, within the first 24 h of wave action, indicating that the wave energy exceeded the emulsification energy threshold; (2) despite notable differences in the hydrocarbon types and contents of the IBP–204 °C fraction among the oils, this light fraction was rapidly lost within the first 24 h, primarily due to evaporation; (3) the density and viscosity of the 24-h water-in-oil (w/o) emulsions increased due to the combined effects of light fraction loss and water uptake; (4) when comparing the 24-h and 96-h w/o emulsions from the same tests, time-dependent changes in viscosity were more significant than changes in density.

HC and ANS oils, characterized by low density, viscosity, and asphaltene and resin content in their fresh state, formed entrained w/o emulsions after being spilled. Emulsions formed from Dilbit, PAC and VLSFO were classified as stable, which had high viscosity and limited dispersion. As the physical and chemical properties of w/o emulsions evolve over time due to weathering processes, understanding the dynamics of oil loss and water uptake is essential. The characterization and stability analyses of those formed w/o emulsions from simulated mesoscale tests provide quantitative dataset and insights for predicting the movement of those spilled oils in marine environments and for evaluating the suitability of different spill response countermeasures. This work highlights the intrinsic correlations between oil viscosity, chemical composition, and emulsification behavior. The data reported in this work would substantially help fill existing spill databases, such as NOAA's ADIOS, and

enhance future spill modeling and prediction for these oils and crudes.

Despite the progress made, questions remain about how heavier oil compounds in BP > 204 °C fraction transform under environmental weathering conditions, including photo-oxidation and biodegradation, following the evaporation and loss of lighter oil fraction (IBP–204 °C fraction). Changes in the concentrations of various subfractions in weathered emulsions could significantly alter their water distribution, physical properties, and stability over time. Further research at mesoscale and field scales, accounting for critical environmental factors including icy temperature, irradiance, microbial activity, and dispersant application, is necessary to improve our understanding and predictive modeling of w/o emulsion behavior and stability in dynamic aquatic environments.

Supplementary Information

The online version contains supplementary material available at https://doi.org/10.1186/s40068-025-00434-2.

Supplementary Material 1

Acknowledgements
The authors would also like to thank the Technical Service Team and the Standard Analytical Lab in CanmetENERGY Devon for their supports.

Author contributions
Qin Xin : Conceptualization, formal analysis, investigation, methodology, funding acquisition, supervision, validation, writing - original draft, writing - review & editing. **Christine Ridenour** : data curation, formal analysis, investigation, resources, supervision, writing - reviewing & editing. **Hena Farooqi** : investigation, project administration, resources, supervision, writing - reviewing & editing.

Funding
The authors acknowledge the Oceans Protection Plan and Marine Conservation Targets funding supports from the Treasury Board of Canada Secretariat.

Data availability
Data are available upon request from the corresponding author.

Declarations

Competing interests
The authors declare no competing interests.

Consent to publication
Not applicable.

Ethics and Consent to Participate
Not applicable.

Received: 9 October 2025 / Accepted: 4 November 2025
Published online: 07 December 2025

References

Abdulredha MM, Hussain SA, Abdullah LC, Hong TL (2022) Water-in-oil emulsion stability and demulsification via surface-active compounds: a review. J Pet Sci Eng 209:109848

Aeppli C, Mitchell DA, Keyes P, Beirne EC, McFarlin KM, Roman-Hubers AT, Nedwed T (2022) Oil irradiation experiments document changes in oil properties, molecular composition, and dispersant effectiveness associated with oil photo-oxidation. Environ Sci Technol 56(12):7789–7799

Daling P, Leirvik F, Almås IK, Brandvik PJ, Hansen BH, Lewis A, Reed M (2014) Surface weathering and dispersibility of MC252 crude oil. Mar Pollut Bull 87(1–2):300–310

de Oliveira MCK, Miranda LRO, de Carvalho ABM, Miranda DFS (2018) Viscosity of water-in-oil emulsions from different American petroleum Institute gravity Brazilian crude oils. Energy Fuels 32(3):2749–2759

Fingas M (2014) Water-in-oil emulsions: formation and prediction. J Petroleum Sci Res 3:38–49

Fingas M, Fieldhouse B (2004) Formation of water-in-oil emulsions and application to oil spill modelling. J Hazard Mater 107(1):37–50

Fingas M, Fieldhouse B (2009) Studies on crude oil and petroleum product emulsions: water resolution and rheology. Colloids Surf A 333:67–81

Fingas M, Fieldhouse B, Mullin J (1999) Studies of water-in-oil emulsions: Energy Threshold of Emulsion Formation, Proceedings of the Twenty-second AMOP Technical Seminar, Environment and Climate Change Canada, Ottawa, ON, Canada, pp. 57–68

Heshka NE et al (2021) High resolution orbitrap mass spectrometry analysis of oxidized hydrocarbons found in freshwater following a simulated spill of crude oil. Chemosphere 292:133415

Hounjet LJ, Xin Q, McDonald R (2023) Bitumen processing reduces diluent content of pipeline-transportable products and can mitigate impacts of spills into various water types. Fuel 331:125826

Lara-Jacobo LR, Gauthier C, Xin Q, Dupont F, Couture P, Triffault-Bouchet G, Dettman HD, Langlois VS (2021) Fate and fathead minnow embryotoxicity of weathering crude oil in a Pilot-Scale spill tank. Environ Toxicol Chem 40(1):127–138

Lee RF (2003) Photo-oxidation and photo-toxicity of crude and refined oils. Spill Sci Technol Bull 8(2):157–162

Li J, Ji W, Prince RC, Lee K, Pegau WS, Boufadel M (2025) Impact of below-freezing air temperatures on the formation and stability of seawater-crude oil emulsion. Mar Pollut Bull 218:118186

Liu, R., Daskiran, C., Mukherjee, A., Xin, Q., Cui, F., Marras, S., Farooqi, H., Dettman H.D.,Boufadel, M (2003) "Characterization and modelling of water mixing energies and particle behavior Q1 Q2 Q3 Q4 Q5 Q6 Q7 Q8 Q9 during wave generation in CanmetENERGY Devon spill test tank". Ocean Engineering 2023, 278, 114237. Formation

Muriel DF, Katz J (2021) Time evolution and effect of dispersant on the morphology and viscosity of water-in-crude-oil emulsions. Langmuir 37:1725–2742

Muriel DF, Katz J (2023) Effects of crude oil properties and dispersant on the microstructure and viscosity of Seawater-in-Oil emulsions. Langmuir 39(5):2043–2062

Muriel DF, Fuentes-Cabrejo C, Escobar-Castaneda N, Katz J (2024) The effects of photo-oxidation, wave energy, and crude oil properties on the microstructure and viscosity of water-in-oil emulsions, *International Oil Spill Conference Proceedings*

Plata, D. L.; Sharpless, C. M.; Reddy, C. M., Photochemical Degradation ofPolycyclic Aromatic Hydrocarbons in Oil Films. Environmental Science & Technology 2008, 42(7), 2432-2438.

Rane JP, Vincent P, Alexander C, Sanjoy B (2013) Interfacial rheology of asphaltenes at Oil-Water interfaces and interpretation of the equation of state. Langmuir 29(15):4750–4759

Royal Society of Canada (2015) Expert Panel Report, Behavior and Environmental Impacts of Crude Oil Released into Aqueous Environments, Ottawa, ON. ISBN: 978-1-928140-02-3

Saborimanesh N, Xin Q, Ridenour C, Farooqi H (2023) Response of Microbial Communities in North Saskatchewan River to Diluted Bitumen and Conventional Crude under Freeze-Thaw-Refreeze Cycle. Environ Pollut 323:121256

Wang D, Yang D, Huang C, Huang Y, Yang D, Zhang H, Liu Q, Tang T, Gamal El-Din M, Kemppi T, Perdicakis B, Zeng H (2021) Stabilization mechanism and chemical demulsification of water-in-oil and oil-in-water emulsions in petroleum industry: a review. Fuel 286:119390

Wong SF, Lim JS, Dol SS (2015) Crude oil emulsion: a review on formation, classification and stability of water-in-oil emulsions. J Petrol Sci Eng 135:498–504

Xin Q, Hounjet LJ, Hartwell A (2022) Spill behaviors of pipeline-transportable processed bitumen products in fresh water. Fuel 309:122040

Xin Q, Saborimanesh N, Greer CW, Dettman HD, Farooqi H (2023) Seasonal Effect on Dynamics of Hydrocarbon Profile and Microbial Community Changes in

North Saskatchewan River Water under Simulated Diluted Bitumen Spill Tank Tests. J Sci Total Environ 859(1):160161
Xin Q, Saborimanesh N, Ridenour C, Farooqi H (2024) Fate, behavior and microbial response of diluted bitumen and conventional crude spills in a simulated warm freshwater environment. Environ Pollut 343:123224
Zhao L, Nedwed T, Daling PS, Brandvik PJ (2022) Investigation of the spreading tendency of emulsified oil slicks on open systems. Mar Pollut Bull 180:113739

Publisher's note